

On fractal properties of the cosmic web

J. Einasto^{1,2,3}, G. Hütsi⁴, T. Kuutma¹, and M. Einasto¹

¹ Tartu Observatory, 61602 Tõravere, Estonia

² Estonian Academy of Sciences, 10130 Tallinn, Estonia

³ ICRA Net, Piazza della Repubblica, 10, 65122 Pescara, Italy

⁴ National Institute of Chemical Physics and Biophysics, Tallinn 10143, Estonia

Received ; accepted

ABSTRACT

Aims. Our goal is to find how the spatial correlation function of galaxies describes the multifractal nature of the cosmic web.

Methods. We calculate spatial correlation functions of galaxies, $\xi(r)$, structure functions, $g(r) = 1 + \xi(r)$, and fractal dimension functions, $D(x) = 3 + \gamma(r) = 3 + d \log g(r) / d \log r$, using dark matter particles of biased Λ cold dark matter (CDM) simulation, observed galaxies of the Sloan Digital Sky Survey (SDSS), and simulated galaxies of the Millennium and EAGLE simulations. We analyse how these functions describe fractal and other geometrical properties of the cosmic web.

Results. Correlation functions of biased Λ CDM model samples describe at small distances (particle/galaxy separations), $r \leq 2.25 h^{-1}$ Mpc, the distribution of matter inside DM halos. In real and simulated galaxy samples only brightest galaxies in clusters are visible, and the transition from clusters to filaments occurs at distance $r \approx 0.8 - 1.5 h^{-1}$ Mpc. On larger separations correlation functions describe the distribution of matter and galaxies in the whole cosmic web. The effective fractal dimension of the cosmic web is a continuous function of the distance (separation). On small separations, $r \leq 2 h^{-1}$ Mpc, the fractal dimension decreases from $D \approx 1.5$ to $D \approx 0$, reflecting the distribution inside halos/clusters. The minimum of the fractal dimension function $D(r)$ near $r \approx 2$ is deeper for more luminous galaxies. On medium separations, $2 \leq r \leq 10 h^{-1}$ Mpc, the fractal dimension grows from ≈ 0 to ≈ 2 , and approaches at large separations 3 (random distribution). Real and simulated galaxies of low luminosity, $M_r \geq -19$, have almost identical correlation lengths and amplitudes, indicating that dwarf galaxies are satellites of brighter galaxies, and do not form a smooth population in voids.

Conclusions. Spatial correlation functions of galaxies contain valuable information on fractal dimension and other geometrical properties of the cosmic web.

Key words. Cosmology: large-scale structure of Universe; Cosmology: dark matter; Cosmology: theory; Galaxies: clusters; Methods: numerical

1. Introduction

According to the presently accepted cosmology paradigm dark matter (DM) is the dynamically dominant population of the universe, and the Λ cold dark matter (CDM) model is a good representative of the true distribution of matter in the universe. The distribution of matter and galaxies in the present epoch forms a very complex structure called the cosmic web. The most commonly used statistic to study the structure of the universe is the two-point correlation function of galaxies. It is a function of distance and describes the excess probability of finding two galaxies separated by this distance. So far correlation functions have been considered as tools to characterise general properties of the distribution of galaxies, and used to search for characteristic scales in galaxy distribution, like the baryonic acoustic oscillation (BAO) scale. In more detailed investigations of the structure of the cosmic web numerous other methods were used, as discussed in a recent symposium on the cosmic web (van de Weygaert et al. 2016).

One aspect of the structure of the cosmic web is its fractal character. The fractal geometry of various objects in nature was discussed by Mandelbrot (1982). The study of fractal properties of the cosmic web has a long history. The first essential step to study fractal properties of the cosmic web was made by

Soneira & Peebles (1978). Authors constructed a fractal model which allows to reproduce the angular correlation function of the Lick catalog of galaxies, as found by Seldner et al. (1977). Over a wide range of mutual separations (distances), $0.01 \leq r \leq 10 h^{-1}$ Mpc, the correlation function can be represented by a power law, $\xi(r) = (r/r_0)^\gamma$, where $r_0 = 4.5 \pm 0.5 h^{-1}$ Mpc is the correlation length, $\gamma = -1.77$ is a characteristic power index, and $D = 3 + \gamma = 1.23 \pm 0.04$ is the fractal dimension of the sample (Peebles 1989, 1998).

Subsequent studies have shown that the cosmic web has actually a multifractal character, as found by numerous authors, starting from Jones et al. (1988), and confirmed by Balian & Schaeffer (1988), Martinez et al. (1990), Einasto (1991b), Guzzo et al. (1991), Colombi et al. (1992) Martinez et al. (1993), Borgani (1995), Mandelbrot (1997), Baryshev et al. (1998), Gaité et al. (1999), Bagla et al. (2008), Chacón-Cardona & Casas-Miranda (2012), Gaité (2018, 2019). In these pioneering studies the fractal character of the web was studied mostly locally in samples of different size, as discussed by Martínez & Saar (2002).

The goal of the present paper is to study global fractal properties of the cosmic web by using spatial correlation functions of galaxies, especially its multifractal character. For this purpose we use as basis a Λ CDM model, calculated in a box of size $512 h^{-1}$ Mpc. The model is calculated using cosmological

Send offprint requests to: J. Einasto, e-mail: jaan.einasto@ut.ee

parameters: Hubble parameter $H_0 = 100h \text{ km s}^{-1} \text{ Mpc}^{-1}$, matter density parameter $\Omega_m = 0.28$, and dark energy density parameter $\Omega_\Lambda = 0.72$. We take advantage of the fact that for this model positions of all particles are known. This allows to compare correlation functions of matter and simulated galaxies. For comparison we analyse absolute magnitude (volume) limited SDSS samples, as found by Liivamägi et al. (2012) and Tempel et al. (2014b). We analyse also absolute magnitude selected galaxy samples from the Millennium simulation by Springel et al. (2005), and galaxy catalogues by McAlpine et al. (2016) of the EAGLE simulation.

It is presently well accepted that galaxies form in DM dominated halos (White & Rees 1978). Thus the spatial correlation function at small separations r characterises the distribution of galaxies within DM dominated halos/clusters, and on larger separations the distribution of galaxies in the whole cosmic web, as shown by Einasto (1991a, 1992), Guzzo et al. (1991), Berlind & Weinberg (2002), Zehavi et al. (2004) and Kravtsov et al. (2004). This leads to departures of the correlation function from the pure power law. To investigate this property of the cosmic web in more details we shall use the correlation function of galaxies, $\xi(r)$, and its derivatives – the structure function, $g(r) = 1 + \xi(r)$, its log-log derivative, the fractal function, $\gamma(r) = d \log g(r) / d \log r$, and the fractal dimension function, $D(x) = 3 + \gamma(r) = 3 + d \log g(r) / d \log r$.

The paper is organised as follows. In the next section we describe simulation and observational data used, methods to calculate correlation functions and its derivatives, and first results of the analysis of these functions for simulated and real galaxy samples of various luminosity limits. In section 3, we study fractal properties of the cosmic web as described by the correlation function and its derivatives. In section 4 we discuss the luminosity dependence of correlation functions and its derivatives of Λ CDM and galaxy samples, and the dependence of correlation functions on the size of the sample, and zero crossing of correlation functions. The last section brings our conclusions.

2. Methods, data and first results

In this section we describe simulation and observational data used and methods to calculate correlation functions. We start with the description of methods to calculate correlation and related functions. Thereafter we describe the Λ CDM numerical simulation used to find density fields at various density threshold levels to simulate galaxy samples of different luminosity. Next we describe our basic observation sample selected from the Sloan Digital Sky Survey (SDSS), and EAGLE and Millennium simulations, used for comparison with observational samples. Finally we describe our first results in the calculation of correlation functions.

2.1. Calculation of correlation functions

Classical methods to calculate angular and spatial correlation functions using catalogs of extragalactic objects were elaborated by Limber (1953, 1954), Totsuji & Kihara (1969), Peebles (1973) and Groth & Peebles (1977), see also Peebles (1980) and Martínez & Saar (2002).

The natural estimator to find the two-point spatial correlation function is:

$$\xi_N(r) = \frac{DD(r)}{RR(r)} - 1, \quad (1)$$

and the Landy & Szalay (1993) estimator

$$\xi_{LS}(r) = \frac{DD(r) - 2DR(r) + RR(r)}{RR(r)}. \quad (2)$$

In these formulae r is the galaxy pair separation (distance), and $DD(r)$, $DR(r)$ and $RR(r)$ are normalised counts of galaxy-galaxy, galaxy-random and random-random pairs at distance r of pair members.

A careful analysis of almost all catalogues, available in 1970s, was performed by Peebles & Hauser (1974a,b); Peebles & Groth (1975); Peebles (1975a,b). These studies showed that the spatial correlation function can be expressed by a simple law: $\xi(r) = (r/r_0)^\gamma$, where $r_0 \approx 5 h^{-1} \text{ Mpc}$ is the correlation length of the sample, and the power index $\gamma \approx -1.7$ is almost the same for all galaxy samples studied (Peebles 1998).

In the present paper we applied the Landy-Szalay estimator for samples of SDSS galaxies, and the natural estimator for cubical EAGLE and Millennium model galaxy samples. Model samples have two scale parameters, the length of the cube, L in $h^{-1} \text{ Mpc}$, and the maximal distance to calculate the correlation function, L_{max} . The second parameter is used to exclude pairs with separations larger than L_{max} in the loop over galaxies to count pairs. This speeds up calculations considerably, so that calculations of correlation functions of samples up to one million galaxies can be done in less than 20 minutes using a MacBook Pro. The separation interval r from 0 to L_{max} was divided into 100 equal bins of length $L_{max}/100$ in case of EAGLE and Millennium samples, and into N_b equal bins of length $\log L_{max}/N_b$ for SDSS samples. Varying L_{max} and N_b we can use different bin sizes, optimal for the particular sample. The core of the Fortran program, used for Millennium and EAGLE samples, was written many years ago to investigate correlation functions of galaxies by Einasto et al. (1986), Klypin et al. (1989) and Einasto et al. (1997a,b). At these times computers were very slow and optimization of programs was crucial. The random-random pair count $RR(r)$ was found applying the random number generator ran2 by Press et al. (1992), using one or two million particles. To speed up the calculation of random-random pairs we split random samples into 10 independent subsamples, as done also by Keihänen et al. (2019).

Λ CDM model samples contain all particles with local density labels $\delta \geq \delta_0$. To find correlation functions of these samples conventional method cannot be used, since the number particles is too large, up to 512^3 in the full unbiased model. To find correlation functions of Λ CDM samples we used in this paper the Szapudi et al. (2005) method. Conventional methods scale as $O(N^2)$. When the number of objects N becomes large, the method is too slow. Measurements of power spectra can be obtained with fast Fourier transforms (FFT), which scale as $O(N \log N)$. The Szapudi et al. (2005) method uses FFT also to calculate correlation functions and scales as $O(N \log N)$. The method is an implementation of the algorithm eSpICE, the Euclidean version of SpICE by Szapudi et al. (2001). As input the method uses density fields on grids 1024^3 , 2048^3 , and 3072^3 . Correlation functions are found with $L_{max} = 100 h^{-1} \text{ Mpc}$, and with 200, 400 and 600 linear bins, respectively.

In the following analysis we use the spatial correlation function, $\xi(r)$, and the pair correlation or structure function, $g(r) = 1 + \xi(r)$, to characterise the distribution of galaxies in space, for details see Martínez & Saar (2002). Instead of the slope of the correlation function as a parameter, γ , we calculate the log-log gradient of the pair correlation function as a function of distance,

$$\gamma(r) = \frac{d \log g(r)}{d \log r}, \quad (3)$$

The $\gamma(r)$ function characterises the effective fractal dimension $D(r)$ of samples at mean separation of galaxies at r ,

$$D(r) = 3 + \gamma(r). \quad (4)$$

We call the $D(r) = 3 + \gamma(r)$ function as the fractal dimension function. Martínez & Saar (2002) defined the correlation dimension $D_2 = 3 + d \log \hat{g}(r) / d \log r$, where $\hat{g}(r)$ is the average of the structure function, $\hat{g}(r) = 1/V \int_0^r g(r') dV$. For our study we prefer to use the local value of the structure function to define its gradient. The effective fractal dimension of a random distribution of galaxies is $D = 3$, and respectively $\gamma = 0$; in sheets $D = 2$ and $\gamma = -1$; in a filamentary distribution $D = 1$ and $\gamma = -2$; within clusters $D = 0$ and $\gamma = -3$.

To find the gradient $\gamma(r)$ of the structure function $g(r)$ we use a linear fit of the structure function. At small distances the function changes very rapidly and we use for its gradient at r just previous and following $\log g(r)$ value divided to \log step size in r . At larger distances we use a linear fit in the distance interval $\pm m$ steps from the particular r value of $\log g(r)$, presented as a table. The fit is found using the `fit` subroutine by Press et al. (1992), which gives the gradient and its error. Correlation functions and their derivatives were calculated with a constant linear or logarithmic step size.

Correlation functions $\xi(r)$, structure functions $g(r) = 1 + \xi(r)$, and fractal dimension functions $D(r) = 3 + \gamma(r)$, are shown in Fig. 1 for all simulated and real galaxy samples. As usual we use the separation r , where the correlation function has unit value, $\xi(r_0) = 1.0$, as the correlation length of the sample, $r = r_0$. We calculated for all samples the value of the correlation function at distance (galaxy separation) $r = 6 h^{-1}$ Mpc, ξ_0 ; this parameter characterises the amplitude of the correlation function. It is complimentary to the correlation radius r_0 .

2.2. Particle-density-selected model samples

Simulations of the evolution of the cosmic web were performed in a box of size $L_0 = 512 h^{-1}$ Mpc, with resolution $N_{\text{grid}} = 512$ and with $N_{\text{part}} = N_{\text{grid}}^3$ particles. The initial density fluctuation spectrum was generated using the COSMICS code by Bertschinger (1995), assuming cosmological parameters $\Omega_m = 0.28$, $\Omega_\Lambda = 0.72$, $\sigma_8 = 0.84$, and the dimensionless Hubble constant $h = 0.73$. To generate initial data we used the baryonic matter density $\Omega_b = 0.044$ (Tegmark et al. (2004b)). Calculations were performed with the GADGET-2 code by Springel (2005).

For all simulation particles and all simulation epochs, we calculated local density values at particle locations, δ , using positions of 27 nearest particles, including the particle itself. Densities were expressed in units of the mean density of the whole simulation. In the study presented here we used particle-density-selected samples at the present epoch. The full Λ CDM model includes all particles. Following Einasto et al. (2019a) we form biased model samples contain particles above a certain limit, $\delta \geq \delta_0$, in units of the mean density of the simulation. As shown by Einasto et al. (2019a) such sharp density limit allows to find density fields of simulated galaxies, which have geometrical properties close to density fields of real galaxies. Particle-density-selected samples are referred to as biased model samples and are denoted as LCDM.*i*, where *i* denotes the particle-density limit δ_0 . The full DM model includes all particles and corresponds to the particle-density limit $\delta_0 = 0$, and therefore it is denoted as LCDM.00. The main data on biased model samples are given in Table 1. We calculated for all samples the correlation length, r_0 , the amplitude of the correlation function at

Table 1. LCDM particle-density-limited models.

Sample	δ_0	$b(\delta_0)$	r_0	ξ_0
(1)	(2)	(3)	(4)	(5)
LCDM.00	0.0	1.000	4.86	0.729
LCDM.05	0.5	1.143	5.75	0.953
LCDM.1	1.0	1.285	6.75	1.203
LCDM.2	2.0	1.447	7.83	1.530
LCDM.3	3.0	1.548	8.47	1.754
LCDM.4	4.0	1.621	8.89	1.924
LCDM.5	5.0	1.677	9.21	2.061
LCDM.7	7.5	1.778	9.77	2.317
LCDM.10	10.0	1.849	10.14	2.507
LCDM.15	15.0	1.952	10.76	2.794
LCDM.20	20.0	2.031	11.20	3.021
LCDM.30	30.0	2.156	11.96	3.402
LCDM.40	40.0	2.257	12.56	3.725
LCDM.50	50.0	2.342	12.56	3.725
LCDM.80	80.0	2.528	14.4	4.662
LCDM.100	100.0	2.626	14.9	5.038

Notes. The columns are: (1) sample name; (2) particle-density limit δ_0 ; (3) bias parameter, calculated from correlation functions of biased models with particle-density limits δ_0 ; (4) correlation length r_0 in h^{-1} Mpc; (5) correlation function amplitude ξ_0 at $r = 6.0 h^{-1}$ Mpc.

$r = 6 h^{-1}$ Mpc, $\xi_0 = \xi(6)$, and the biasing parameter,

$$b(r, \delta_0) = \sqrt{\xi(r, \delta_0) / \xi(r, 0)}, \quad (5)$$

all as functions of the particle density limit, δ_0 .

The gradient of the pair correlation function changes at small r very rapidly. For this reason we calculated correlation functions using two resolutions, 3072 and 1024. Fractal dimension functions were calculated for the LCDM sample with resolution 3072 with different $\pm m$ steps: for $r \leq 6.5 h^{-1}$ Mpc $m = 3$, for $6.5 < r \leq 17 h^{-1}$ Mpc $m = 10$, and thereafter $m = 50$. In case of the LCDM sample with resolution 1024 we used at $4.5 \leq r \leq 25 h^{-1}$ Mpc $m = 8$, thereafter $m = 25$. The final fractal dimension function presented in Fig. 1 is a combined function, found using the high-resolution field 3072 at small distances, $r \leq 8 h^{-1}$ Mpc, and the field 1024 at larger distances.

LCDM model samples are based on all particles of the simulation, and contain detailed information on the distribution of matter in regions of different density. Top panels of Fig. 1 show correlation functions, $\xi(r)$, structure functions, $g(r) = 1 + \xi(r)$, and fractal dimension functions, $D(r) = 3 + \gamma(r)$, for basic samples of the model.

The first impression from the Figure is: the amplitude of correlation and structure functions continuously increases with the increase of the particle density threshold δ_0 of models. This increase can be expressed by the amplitude parameter ξ_0 , given in Table 1. The radius r_z where correlation function becomes negative is equal to $r_z \approx 80 h^{-1}$ Mpc for all LCDM samples.

2.3. SDSS galaxy samples

We use luminosity limited (usually referred to as volume-limited) galaxy samples by Tempel et al. (2014b), selected from data release 12 (DR12) of the SDSS galaxy redshift survey (Ahn et al. 2014). SDSS galaxy survey has complex footprint in sky. To make computation of reference random samples easier we used a simplified footprint of the survey with limits in survey coordinates $-33^\circ \leq \eta \leq 36^\circ$, $-48^\circ \leq \lambda \leq 51^\circ$.

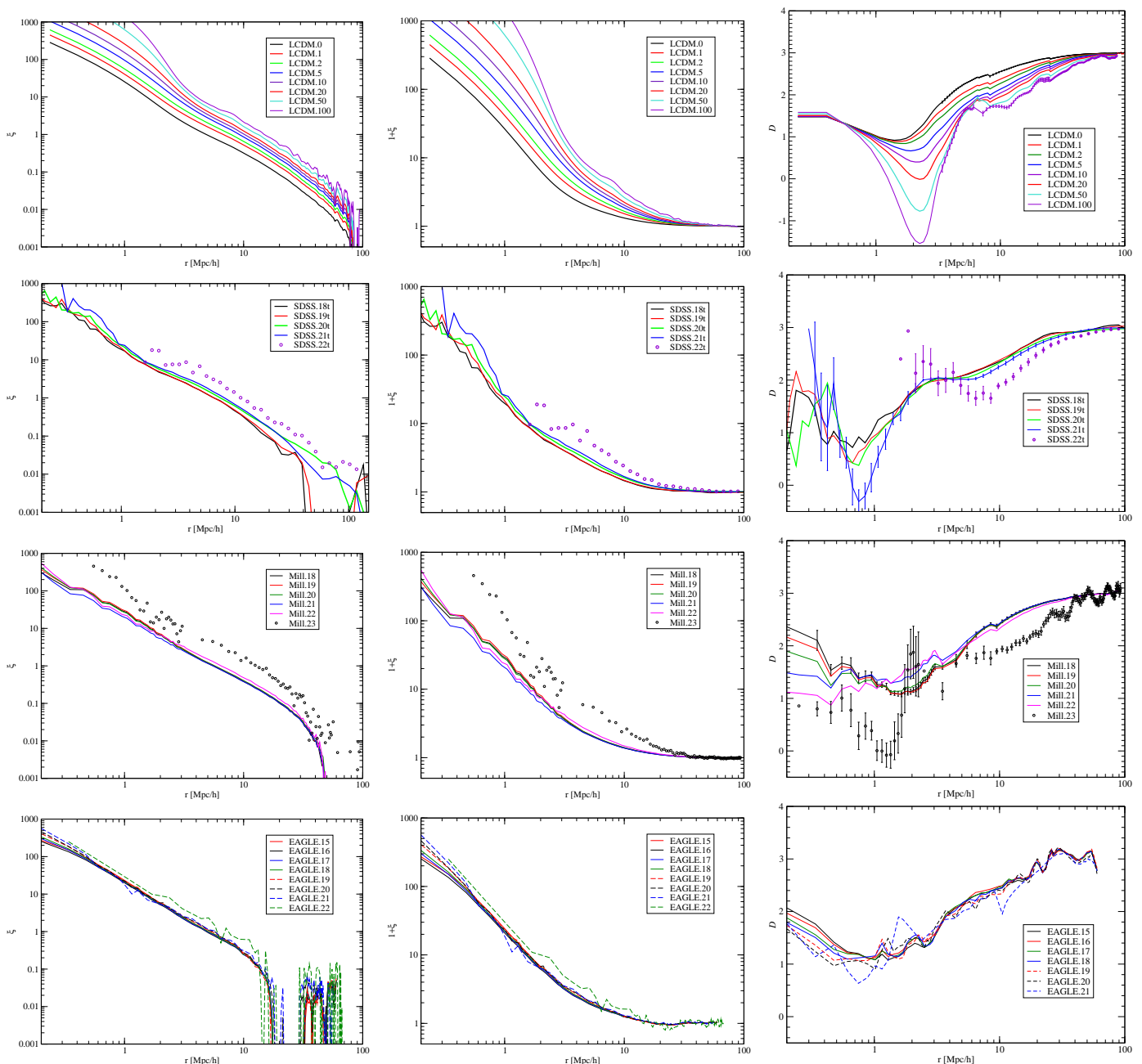


Fig. 1. *Left panels:* correlation functions of galaxies, $\xi(r)$; *middle panels:* pair correlation or structure functions, $g(r) = 1 + \xi(r)$; *right panels:* fractal dimension functions, $D(r) = 3 + \gamma(r)$. *Panels from top to bottom* are: for LCDM models for different particle selection limits; for SDSS galaxies using five luminosity threshold; for six luminosity bins of Millennium galaxies, and for eight luminosity thresholds of EAGLE galaxies. Errors of fractal dimension functions, found with the fit procedure, are given for several representative samples.

Data on five luminosity-limited SDSS samples are given in Table 2: limiting absolute magnitudes in red r -band, M_r , maximum comoving distances, d_{\max} , and numbers of galaxies in samples, N_{gal} . All SDSS samples have minimum comoving distance, $d_{\min} = 60 h^{-1} \text{Mpc}$. SDSS samples with $M_r - 5 \log h$ luminosity limits -18.0 , -19.0 , -20.0 , -21.0 , and -22.0 are referred to as SDSS.18i, SDSS.19i, SDSS.20i, SDSS.21i and SDSS.2i with additional index i , where $i = b$ is for luminosity bins samples, and $i = t$ is for luminosity threshold samples. In luminosity bin samples the width of the bin is one mag, $\Delta M = 1.0$, in luminosity threshold samples the upper limit $M_r - 5 \log h = -25.0$ exceeds the luminosity of the brightest galaxies in the SDSS sample. Respective luminosity limits in solar units were calculated

using the absolute magnitude of the Sun in r -band, $M_{\odot} = 4.64$ (Blanton & Roweis 2007). Table 2 also provides the correlation radius of samples, r_0 , and the value of the correlation function at $r = 6 h^{-1} \text{Mpc}$, ξ_0 , used to characterise the amplitude of the correlation function.

SDSS galaxy samples are conical shells, and corresponding random particle samples were calculated using identical conical shell configurations. Correlation functions of SDSS galaxy samples were calculated using the Landy-Szalay estimator and applying a Python program. SDSS samples differ from model samples in one important aspect. We use absolute magnitude limited samples, but observational samples are flux-limited. For this reason for faintest galaxies only the nearby region with distance

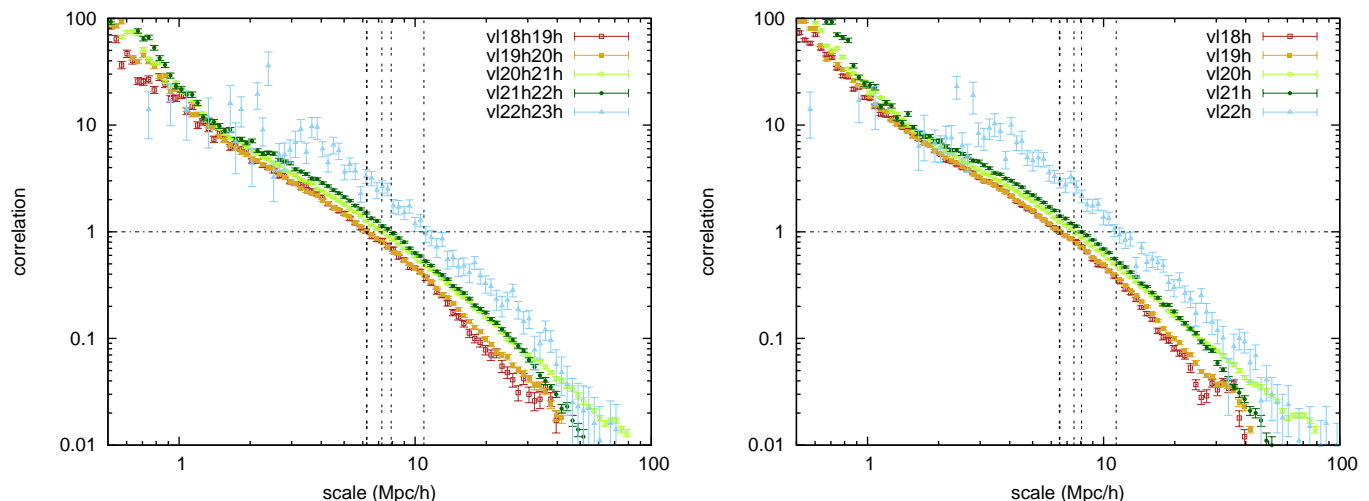


Fig. 2. Comparison of correlation functions of SDSS samples found for absolute magnitude bins and thresholds, left and right panels, respectively. Error bars are shown.

Table 2. SDSS luminosity limited samples.

Sample	M_r	N_{gal}	d_{max}	r_0	ξ_0
(1)	(2)	(3)	(4)	(5)	(6)
SDSS.18b	-18.0	16 676	135	6.41 ± 0.42	1.108
SDSS.19b	-19.0	49 963	211	6.31 ± 0.24	1.100
SDSS.20b	-20.0	105 088	323	7.20 ± 0.19	1.359
SDSS.21b	-21.0	98 674	486	7.93 ± 0.21	1.599
SDSS.22b	-22.0	9 430	571	11.45 ± 0.99	3.304
SDSS.18t	-18.0	39 711	135	6.55 ± 0.28	1.156
SDSS.19t	-19.0	88 132	211	6.56 ± 0.19	1.165
SDSS.20t	-20.0	134 431	323	7.46 ± 0.17	1.447
SDSS.21t	-21.0	104 512	486	8.14 ± 0.21	1.675
SDSS.22t	-22.0	9 525	571	11.32 ± 0.97	3.444

Notes. The columns are: (1) sample name; (2) absolute r -magnitude limit, $M_r - 5 \log h$; (3) number of galaxies in a sample; (4) maximum comoving distance d_{max} in h^{-1} Mpc; (5) correlation length of the sample r_0 in h^{-1} Mpc; (6) correlation function amplitude ξ_0 at $r = 6 h^{-1}$ Mpc.

limit $d_{\text{max}} = 135 h^{-1}$ Mpc can be used, in contrast to the most luminous sample with distance limit $d_{\text{max}} = 571 h^{-1}$ Mpc. The near limit is the same for all samples, $d_{\text{min}} = 60 h^{-1}$ Mpc. SDSS galaxy samples are conical and have different sizes: for example the volume of the sample SDSS.21 is about 50 times larger than the volume of the sample SDSS.18.

To find the behaviour of the correlation function on small distances, it was found on distances $0.1 \leq r \leq 1 h^{-1}$ Mpc using $N_B = 20 \log$ bins, and on scales $0.5 \leq r \leq 200 h^{-1}$ Mpc using $N_B = 45 \log$ bins. The fractal dimension function was calculated using the `fit` subroutine with $m = 2$ on small distances, $r \leq 1 h^{-1}$ Mpc, and $m = 4$ on larger distances.

Correlation functions of SDSS galaxies are shown in Fig. 1 for luminosity threshold, and in Fig. 2 for luminosity bins and thresholds. Correlation functions for luminosity bins are very similar to correlation functions for luminosity thresholds, only correlation lengths are slightly lower, see Table 2. This is expected, since in threshold limited samples brighter galaxies are included which have larger correlation lengths.

The radius r_z where correlation function becomes negative is equal for SDSS.18 and SDSS.19 samples $r_z \approx 45 h^{-1}$ Mpc, for

brighter galaxies it lies higher, $r_z \approx 120 h^{-1}$ Mpc. This difference is expected, since sizes of samples for fainter galaxies are small and cannot be considered as fair samples of the universe. The structure function $g(x) = 1 + \xi(r)$ continuously decreases with increasing distance r .

2.4. Millennium simulation galaxy samples

We used simulated galaxy catalogues by Croton et al. (2006), calculated by semi-analytical models of galaxy formation from Millennium simulations by Springel et al. (2005). The Millennium catalogue contains 8 964 936 simulated galaxies, with absolute magnitudes in r color $M_r \leq -17.4$. Magnitudes are in standard SDSS filters, not in $-5 \log h$ units. For the present analysis we extracted the following data: x, y, z -coordinates, and absolute magnitudes in r and g photometric systems. Millennium samples with M_r luminosity limits $-18.0, -19.0, -20.0, -20.5, -21.0, -21.5, -22.0$ and -23.0 are referred to as Mill.18i, Mill.19i, Mill.20i, Mill.20.5i, Mill.21i, Mill.21.5i, Mill.22i, and Mill.23i, where index $i = b$ is for luminosity bin samples, and $i = t$ is for luminosity threshold samples with upper limit -25.0 . Data on Millennium luminosity limited samples are given in Table 3, including correlation lengths found for Millennium galaxy samples, and the value of the correlation function at $r = 6 h^{-1}$ Mpc, ξ_0 .

The Millennium sample of simulated galaxies has almost 9 million objects. Our first task is how to calculate correlation functions for such large dataset. We tried several possibilities – to divide the sample into smaller subsamples of size 100 and $250 h^{-1}$ Mpc, and to use smaller luminosity bins. Our experience shows that using boxes of size 250 and $500 h^{-1}$ Mpc yields almost identical results for the correlation function. The sample of size $100 h^{-1}$ Mpc contains too few galaxies which leads to larger random and some systematic errors.

One possibility to reduce the size of galaxy samples is to use smaller magnitude bins. We tried at the low end of the luminosity range bins of size 0.15, 0.25 and 0.5 in absolute magnitude. Results for the correlation function are practically identical. We used for samples Mill.18b and Mill.19b luminosity bins 0.25 and 0.50 mag respectively, and for brighter samples bins of size 1.0 mag. Samples with threshold magnitudes at low absolute magnitudes are so big that our program to find correlation function was

Table 3. Millennium luminosity limited galaxy samples.

Sample	M_r	N_{gal}	r_0	ξ_0
(1)	(2)	(3)	(4)	(5)
Mill.18b	-18.0	829 725	5.45 ± 0.05	0.907
Mill.19b	-19.0	1 022 303	5.70 ± 0.03	0.954
Mill.20b	-20.0	1 209 900	5.60 ± 0.04	0.955
Mill.21b	-21.0	568 705	5.44 ± 0.06	0.902
Mill.22b	-22.0	98 575	6.54 ± 0.18	1.176
Mill.23b	-23.0	5 414	12.8 ± 1.46	3.574
Mill.20.0t	-20.0	1 882 809	5.79 ± 0.04	0.952
Mill.20.5t	-20.5	1 183 825	5.81 ± 0.04	0.956
Mill.21.0t	-21.0	672 909	5.81 ± 0.06	0.956
Mill.21.5t	-21.5	309 580	6.13 ± 0.09	1.033
Mill.22.0t	-22.0	104 204	6.84 ± 0.18	1.271
Mill.23.0t	-23.0	5 629	12.9 ± 1.44	3.766

Notes. The columns are: (1) sample name; (2) absolute r -magnitude interval, M_r ; (3) number of galaxies in a sample; (4) correlation length of the sample r_0 in h^{-1} Mpc; (5) correlation function amplitude at ξ_0 .

not able to manage the file. For this reason we calculated correlation functions for magnitude thresholds only for samples with $M_r \leq -20.0$. Results are given in Table 3. In Fig. 1 we show the correlation function, $\xi(r)$, the structure function, $1 + \xi(r)$, and the fractal dimension function, $D(r) = 3 + \gamma(r)$ for luminosity bins. The number of simulated galaxies in most magnitude bin samples is so large, that correlation functions are very smooth with almost no scatter, thus it is easy to find the correlation length r_0 and the amplitude parameter ξ_0 of samples by linear interpolation. As usual, the correlation length is defined as the distance, at which the correlation function has the unit value, $\xi(r_0) = 1.0$. At this distance the central galaxy has just one neighbour, and the density of galaxies is twice the mean density.

Calculations of correlation functions were made with three resolutions, on distances $0.1 \leq r \leq 10 h^{-1}$ Mpc, $1 \leq r \leq 100 h^{-1}$ Mpc, and $2 \leq r \leq 200 h^{-1}$ Mpc, all with $N_b = 100$ equal linear bins of size 0.1, 1, and $2 h^{-1}$ Mpc, respectively. Correlation functions presented in Fig. 1 are results, combined from resolutions with bin sizes 0.1 and $1 h^{-1}$ Mpc, used for $r \leq 3$ and $r > 3 h^{-1}$ Mpc, respectively. To find the fractal dimension function we applied smoothing with $m = 3$ up to $r = 10 h^{-1}$ Mpc, and $m = 6$ on larger distances.

Our calculation show that the correlation function of Millennium galaxies has at small and medium distances a continuously changing slope $\gamma(r)$, as found for SDSS samples. At larger distances the correlation function bends and crosses the zero value, $\xi(r_z) = 0$. The radius r_z where correlation function becomes negative lies at $r_z = 46 \pm 1 h^{-1}$ Mpc for all samples, see Fig. 1.

On large scales $r \geq r_z$ the correlation function lies close to zero value. However, the baryonic acoustic oscillation (BAO) peak at $r \approx 110 h^{-1}$ Mpc is clearly visible, when the function is expanded in vertical direction, as shown in Fig. 3.

2.5. EAGLE simulation galaxy samples

EAGLE (Evolution and Assembly of Galaxies and their Environments) is a suite of cosmological hydrodynamical simulations that follow the formation and evolution of galaxies. Its goals are described by Schaye et al. (2015) and Crain et al. (2015). We extracted galaxy data from the public release of halo and galaxy catalogues (McAlpine et al. 2016). EAGLE simula-

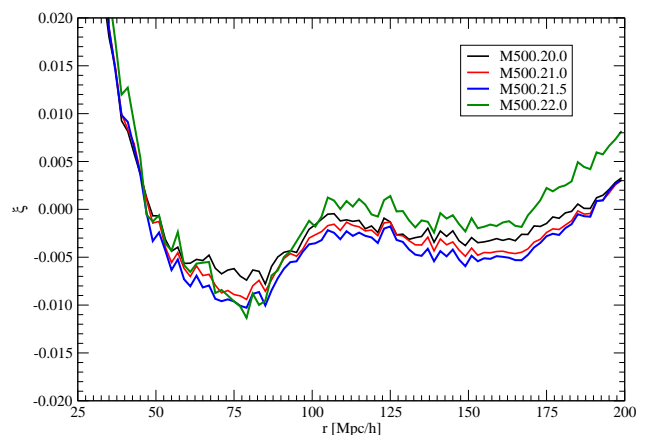


Fig. 3. Correlation functions on large scales of Millennium simulations for luminosity thresholds to see BAO peak at $r \approx 110 h^{-1}$ Mpc.

tions were run with following cosmological parameters: $\Omega_m = 0.308$, $\Omega_\Lambda = 0.692$, $H_0 = 67.8$ km/s per Megaparsec. Within the EAGLE project several simulations were run, we used for the correlation analysis the simulation within a box of comoving size $L = 100$ Mpc. Note that contrary to convention, box sizes and lengths are not quoted in units of $1/h$. This means, that in conventional units the size of the simulation box in comoving coordinates is $L = 67.8 h^{-1}$ Mpc. For the present analysis we used x, y, z -coordinates, and absolute magnitudes in r and g photometric systems.

Table 4. EAGLE luminosity limited samples.

Sample	M_r	N_{gal}	r_0	ξ_0
(1)	(2)	(3)	(4)	(5)
EAGLE.16b	-16.0	7 887	4.72 ± 0.45	0.628
EAGLE.17b	-17.0	5 553	4.81 ± 0.54	0.665
EAGLE.18b	-18.0	4 088	4.72 ± 0.62	0.684
EAGLE.19b	-19.0	3 025	5.15 ± 0.79	0.769
EAGLE.20b	-20.0	2 122	5.35 ± 0.98	0.847
EAGLE.21b	-21.0	987	5.02 ± 1.34	0.789
EAGLE.22b	-22.0	204	6.45 ± 3.79	0.868
EAGLE.16t	-16.0	23 881	4.86 ± 0.26	0.703
EAGLE.17t	-17.0	15 994	4.95 ± 0.33	0.736
EAGLE.18t	-18.0	10 441	5.04 ± 0.41	0.772
EAGLE.19t	-19.0	6 353	5.36 ± 0.56	0.837
EAGLE.20t	-20.0	3 328	5.36 ± 0.78	0.891
EAGLE.21t	-21.0	1 206	5.85 ± 1.42	0.907
EAGLE.22t	-22.0	219	7.46 ± 4.23	0.868

Notes. The columns are: (1) sample name; (2) absolute r -magnitude interval, M_r ; (3) number of galaxies in a sample; (4) correlation length of the sample r_0 in h^{-1} Mpc; (5) correlation function amplitude at ξ_0 .

EAGLE samples with M_r luminosity limits -15.0 , -16.0 , -17.0 , -18.0 , -19.0 , -20.0 , -21.0 , and -22.0 are referred to as EAGLE.15i, EAGLE.16i, EAGLE.17i, EAGLE.18i, EAGLE.19i, EAGLE.20i, EAGLE.21i and EAGLE.22i, where index $i = b$ is for luminosity bin samples of bin size 1.0 mag, and $i = t$ is for luminosity threshold samples with upper limit $M_r - 5 \log h = -25.0$. Data on EAGLE luminosity limited samples are given in Table 4. We give here also correlation lengths found for EAGLE galaxy samples, and the value of the correlation function at $r = 6 h^{-1}$ Mpc, ξ_0 .

For the correlation analysis we used the largest simulated galaxy sample with 29 730 objects in the M_r luminosity interval $-14.7 \geq M_r \geq -23.7$. This allows to calculate correlation functions for luminosity bins and luminosity threshold limits starting from $M_r = -15.0$ up to $M_r = -22.0$. Data on samples are given in Table 4. Correlation, structure and fractal dimension functions are presented in Fig. 1 for luminosity thresholds. Distance scale is expressed in h^{-1} Mpc.

Correlation functions of EAGLE samples were calculated for two resolutions – on distances $0.2 \leq r \leq 20$ Mpc and $1 \leq r \leq 100$ Mpc, with $N_b = 100$ equal linear bins of size 0.2 and 1 Mpc, respectively. Correlation functions are presented in Fig. 1. High resolution functions were used up to distance $r \leq 3 h^{-1}$ Mpc, low resolution functions on larger distances. To find the fractal dimension function we applied smoothing with $m = 3$ up to $r = 3 h^{-1}$ Mpc, and $m = 15$ on larger distances.

The shape of correlation functions is similar to those for the Millennium simulation. The basic difference is that for EAGLE simulation it was possible to find correlation functions for much fainter samples up to $M_r = -15.0$. The radius r_z where correlation function becomes negative is equal for all samples $r_z = 17 \pm 1 h^{-1}$ Mpc, much smaller than for SDSS, LCDM and Millennium samples. This is due to small volume of the simulation box.

2.6. Error estimations of correlation functions

Sampling errors found by bootstrap method for SDSS samples are shown in Fig. 2 for absolute magnitude bin and threshold samples, left and right panels. From these data we found also errors of the correlation length, r_0 , given in Table 2. We found that sampling errors can be approximately expressed as follows: $\epsilon(r_0) = a \times r_0 / \sqrt{N}$, where N is the number of galaxies in the sample, and a is a constant. Similar behaviour have errors of the correlation lengths of SDSS galaxies as found by Zehavi et al. (2011). A similar relation can be used also for errors of correlation function amplitudes, ξ_0 . Using our and Zehavi et al. (2011) SDSS samples we found for the parameter the value, $a = 8.4$. Using this relation we estimated errors of correlation lengths of Millennium and EAGLE simulation samples, given in Tables and in Fig. 7. Relative errors of correlation amplitudes are equal to relative errors of correlation lengths, as given in Fig. 7.

Most our samples contain so many galaxies that random sampling errors are very small, and correlation and structure functions are very smooth. For this reason the scatter of correlation lengths, r_0 , and correlation amplitudes, ξ_0 , found for various luminosity limits of identical samples is also small, see Tables 1 to 3. Relative sampling errors of the correlation length, r_0 , and the correlation amplitude, ξ_0 , are of the order of a few per cent for most samples. Samples corresponding to luminous galaxies contain less objects, thus random sampling errors of r_0 and ξ_0 are larger.

The number of galaxy-galaxy pairs at large distances is very large, as is also the number of random-random pairs. Correlation functions are calculated from ratios of very large almost identical numbers. For this reason sampling errors of correlation functions on large distances are larger, and larger smoothing was needed to calculate correlation dimension functions.

3. Fractal properties of the cosmic web

In this section we discuss fractal properties of the cosmic web as measured by the correlation function and its derivatives. LCDM

samples differ from SDSS, Millennium and EAGLE samples in one principal factor — in LCDM samples individual DM particles are present, in real and simulated galaxy samples only galaxies are present. This difference influences correlation functions and their derivatives, structure and fractal functions. The largest difference is in fractal dimension functions, which do contain information on the distribution of DM particles within halos, as well as on the distribution of DM halos and galaxies in the cosmic web.

3.1. Fractal dimension properties of LCDM models

Einasto (1991a, 1992) and Guzzo et al. (1991) showed that at separations $r < 3 h^{-1}$ Mpc the correlation function of galaxies reflects the distribution of galaxies in groups and clusters, and at larger distances the intracluster distribution (up to $\sim 30 h^{-1}$ Mpc). This was confirmed by Berlind & Weinberg (2002), Zehavi et al. (2004) and Kravtsov et al. (2004), who noticed that at small mutual separations r the correlation function characterises the distribution of matter within DM halos, and on larger separations the distribution of halos (authors of these studies never use the term “cosmic web” to describe the structure of the universe). At the small separation region the spatial correlation function of LCDM model samples is proportional to the density of matter, and measures the density profile inside DM halos. The upper right panel of Fig. 1 shows that the fractal dimension function of LCDM samples depends strongly on the particle density limit δ_0 used in the selection of particles for the sample.

All LCDM samples at the distance $r = 0.5 h^{-1}$ Mpc have identical value of the gradient of structure function, $\gamma(0.5) = -1.5$ and respective local fractal dimension, $D(0.5) = 1.5$. At a distance around $2 h^{-1}$ Mpc gradients have a minimum, depending on the particle density limit δ_0 of samples. For the sample with all particles LCDM.00 the fractal function has a minimum, $\gamma(1.41) = -2.08$ ($D(1.41) = 0.92$) at $r = 1.41 h^{-1}$ Mpc. With increasing particle density limit δ_0 the minimum shifts to larger distances and lower values. For the sample LCDM.10 the minimum is $\gamma(2.08) = -2.60$ ($D(2.08) = 0.40$) at $r = 2.08 h^{-1}$ Mpc, for the sample LCDM.20 it is $\gamma(2.25) = -3.01$ ($D(2.25) = -0.01$) at $r = 2.25 h^{-1}$ Mpc, for the sample LCDM.50 $\gamma(2.25) = -3.77$ ($D(2.25) = -0.77$) at $r = 2.25 h^{-1}$ Mpc, and for the sample LCDM.100 $\gamma(2.25) = -4.54$ ($D(2.25) = -1.54$) at $r = 2.25 h^{-1}$ Mpc. After the minimum the fractal function increases and reaches at largest distance the expected value, $\gamma(100) \approx 0$ ($D(100) \approx 3.0$), for all samples.

The presence of a minimum of the fractal function at small distances is expected. It is well-known that DM halos have almost identical DM density profiles, which can be described by the NFW (Navarro et al. 1996) and by the Einasto (1965) profile. As shown by Wang et al. (2019), the density of DM halos is better fitted by the Einasto profile

$$\rho(r) = \rho(0) \exp\left[-\frac{2}{\alpha} \left(\frac{r}{r_{-2}}\right)^\alpha\right], \quad (6)$$

where r_{-2} is the radius at which the logarithmic slope is -2 , $\rho(0)$ is the central density, and α is a shape parameter. Wang et al. (2019) showed that density profiles of halos of very different mass are almost identical over a very large range of halo masses, and have the shape parameter value $\alpha = 0.16$. Authors calculated the logarithmic density slope $d \log \rho / d \log r$ of the density profile over a distance range $0.05 \leq r/r_{-2} \leq 30$. At $r/r_{-2} = 0.2$ the logarithmic slope is $d \log \rho / d \log r = -1.5$, and decreases to $d \log \rho / d \log r = -3.0$ at $r/r_{-2} = 10$.

At small distances correlation functions are mean values of sums of particle mutual distances within DM halos, averaged over the whole volume of samples. In the full sample LCDM.00 small DM halos dominate, and the minimum of the fractal dimension function $D(r) = 3 + \gamma(r)$ has a moderate depth. With increasing particle density limit δ_0 low-density halos are excluded from the sample and more massive halos dominate. This leads to the increase of the depth of the minimum of $\gamma(r)$ and $D(r)$ functions. More massive halos have larger radii, thus the location of the minimum of the $D(r) = 3 + \gamma(r)$ function shifts to higher distance r values. More massive halos have also higher density, thus the minimum of the $D(r) = 3 + \gamma(r)$ function is deeper. The r value of minimum can be considered as the effective radius of dominating DM halos of the sample.

After the minimum at larger r values the distribution of DM particles outside halos dominates. This leads to the increase of the $D(r) = 3 + \gamma(r)$ function. In these regions the distribution of DM particles of the whole cosmic web determines the correlation function and its derivatives. The transition from one DM halo to the general cosmic web occurs at $r \approx 2.25 h^{-1}$ Mpc, in good agreement with characteristic sizes DM halos.

We conclude that correlation functions of our biased LCDM models describe in a specific way fractal dimension properties of DM halos as well as fractal dimension properties of the whole cosmic web.

3.2. Fractal dimension properties of galaxy samples

SDSS samples have at lowest r values a large scatter of $\gamma(r)$ and $D(r)$ functions. This is due to the very small number of galaxies at such small separations. The mean value of the fractal dimension function is about 1.5, similar to the value for LCDM samples. With increasing distance r the $\gamma(r)$ and $D(r)$ functions decrease, and have a minimum around $r \approx 0.8 h^{-1}$ Mpc. The minimum is deeper for brightest galaxies of the sample SDSS.21. Thereafter with increasing r the $\gamma(r)$ and $D(r)$ functions increase rapidly up to $D(3) \approx 2$, which correspond to fractal dimensions of sheets. At still larger distance between galaxy pairs r the $\gamma(r)$ function approaches smoothly a value $\gamma(r) = 0$ at large r , as expected for a random distribution of galaxies with a fractal dimension $D = 3$.

Fractal functions of Millennium and EAGLE simulation samples start at low r -values at $\gamma(r) \approx -1.5$, $D(r) \approx 1.5$, also with a large scatter. For both simulated galaxy samples the fractal dimension function has a minimum at $r \approx 1.5 h^{-1}$ Mpc. The minimum is deeper for brighter galaxies. It follows a gradual increase of the fractal dimension up to $D = 3$ at large distance.

Fractal dimension functions of LCDM and galaxy samples differ in one important detail — the transition from halos/clusters to web for luminous galaxies occurs at different scales, $r \approx 2.25 h^{-1}$ Mpc for LCDM models, $r \approx 0.8 h^{-1}$ Mpc for real galaxies, and $r \approx 1.5 h^{-1}$ Mpc for simulated galaxies. This small difference shows that the internal structure of DM halos of LCDM models differs from the internal structure of clusters of galaxies. In our biased LCDM model samples all DM particles with density labels $\delta \geq \delta_0$ are present. Thus we see the whole density profile of clusters up to the outer boundary of the halo at δ_0 level. In both real and simulated galaxy samples only galaxies brighter than the selection limit are present. This means that in most luminous galaxy samples only one or few brightest galaxies are located within the visibility window, and the true internal structure of clusters up to their outer boundary is invisible. This difference is larger for real galaxies.

This result is valid not only for rich clusters of galaxies. Ordinary galaxies of the type of our Galaxy and M31 are surrounded by satellite galaxies like Magellanic Clouds and dwarf galaxies around the Galaxy, and M32 and dwarfs around M31. According to available data all ordinary galaxies have such satellite systems (Einasto et al. 1974b; Wechsler & Tinker 2018). However, most satellites have so low luminosity that they are invisible in galaxy surveys like SDSS. For this reason the distribution of DM and visible matter within Galaxy type halos is different, as noticed already in the early study by Einasto et al. (1974a). Groups and clusters of galaxies have more bright member galaxies, but at large distances fainter members of groups become also invisible. Thus with increasing distance the number of visible galaxies in clusters decreases, and on large distance only the brightest galaxy has the luminosity high enough to fall into the visibility window of the survey, see Fig. 9 of Tempel et al. (2009).

Cross sections of spatial 3D density fields of SDSS and LCDM samples are shown in Fig. 14 of Einasto et al. (2019a). Over the whole area of cross sections of 3D fields there exist small isolated spots. These spots correspond to primary galaxies of groups (clusters), where satellite galaxies lie outside the visibility window, or the number of members in groups is considerably reduced. In the calculation of correlation functions these groups enter as isolated galaxies of the field without any nearby galaxies, or to groups with only a few member-galaxies.

The difference in spatial distribution of galaxies and matter in sub-megaparsec scales is the principal reason of the difference between correlation functions of LCDM and SDSS samples on small separations. Visible matter in Galaxy type halos is concentrated to the central main galaxy, satellite galaxies have so low luminosities, that they contribute little to the distribution of luminous matter. In contrast, DM has a smooth distribution within the halos over the whole volume of the halo up to its outer boundary.

3.3. Fine details of fractal dimension functions

Correlation functions of LCDM models with highest particle selection limit δ_0 have a bump at $r \approx 8 h^{-1}$ Mpc, which causes small wiggles in the fractal dimension function. These wiggles are probably related to the distribution of galaxies and groups along filaments. A classical example is the Perseus-Pisces supercluster. As shown by Jõeveer et al. (1977, 1978), clusters and groups of galaxies along the main chain of the Perseus-Pisces supercluster are located at regular intervals of about $7 h^{-1}$ Mpc. The same characteristic distance was found by Tempel et al. (2014a) in the distribution of clusters/groups in SDSS galaxy filaments.

Correlation functions of most luminous galaxies have a small bump at $r \approx 3 h^{-1}$ Mpc. These local features of the correlation function are reasons for the presence of wiggles of the fractal dimension functions between $2 \leq r \leq 10 h^{-1}$ Mpc. The local bump at $r \sim 2-3 h^{-1}$ Mpc can be an evidence of the splashback feature in the halo/cluster profile. This feature is seen in the halo density profile as a sharp decline of its slope at halo boundaries, and is used to define halo/cluster boundaries (Diemer & Kravtsov 2014). Observationally, splashback features have been detected in cluster density profiles, as found among others by Baxter et al. (2017), Chang et al. (2018), and Shin et al. (2019).

Fractal dimension functions of Millennium and EAGLE samples have at distances $r > 20 h^{-1}$ Mpc several wiggles for most luminous galaxy samples. These wiggles are due to relative locations of rich clusters of galaxies. In larger samples mutual distances of rich clusters are more randomised and wiggles

are levered out. In this respect correlation functions act as geometrical functions, as discussed by Einasto et al. (1997b).

These local features are seen only in samples of most luminous galaxies and highly biased LCDM samples. Less massive clusters/halos have smoother profiles and distributions, and these features are hidden in the large body of all galaxies.

4. Luminosity dependence and other properties of LCDM and galaxy samples

In this section we discuss the luminosity dependence of correlation functions and its derivatives of LCDM and galaxy samples, and bias parameters, found for these samples. Next we study the dependence of correlation functions on the size of the sample, and zero crossing of correlation functions. We focus the discussion on differences of correlation properties of samples with real or simulated galaxies and with DM particles only.

4.1. Luminosity dependence of correlation functions of SDSS and LCDM samples

The luminosity dependence of correlation functions is the principal factor of the biasing phenomenon, as discussed by Kaiser (1984). Using recent data the luminosity dependence was studied in detail by Norberg et al. (2001), Tegmark et al. (2004a) and Zehavi et al. (2005, 2011). Here we shall compare the luminosity dependence of correlation functions of real and simulated galaxies, as found in the present analysis.

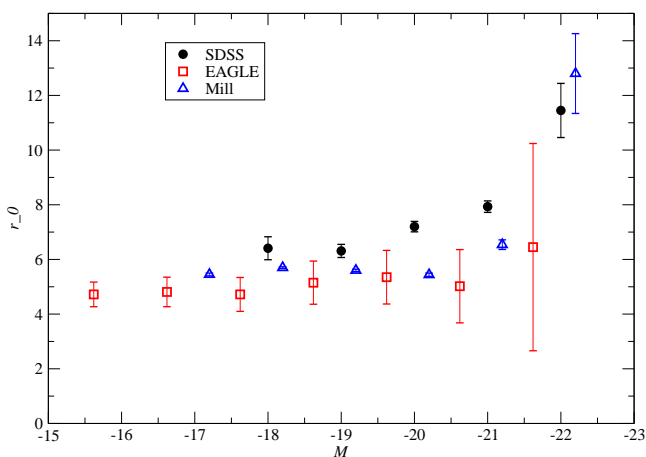


Fig. 4. Correlation length r_0 of SDSS galaxies. For comparison also correlation lengths of EAGLE and Millennium simulations are given, all for luminosity bins.

Our first task is to compare clustering properties of real SDSS galaxy samples with clustering properties of simulated galaxies of EAGLE and Millennium simulations. To compare correlation functions of simulated and real samples, simulated galaxy data must be reduced to real galaxy data in terms of spatial densities. We found spatial densities of galaxies for all SDSS, EAGLE and Millennium subsamples for various luminosity limit. The comparison of densities shows that in order to bring spatial densities of simulated galaxies to the same density level as SDSS galaxies, absolute magnitude limits of EAGLE simulation samples are to be shifted toward fainter limits by 0.38 mag, and of Millennium simulation samples by 0.80 mag. To get identical spatial densities the shift is slightly magnitude dependent, but we ignore this difference and use identical shifts for all samples of galaxies of the same simulation.

In Fig. 4 we show correlation lengths, r_0 , of SDSS, EAGLE and Millennium samples as functions of the magnitude M_r . We see that the correlation length r_0 has a rather similar luminosity dependence for all samples. Correlation lengths and amplitudes of SDSS samples are a bit higher than in simulated galaxy samples, by a factor of about 1.2.

An important detail in the luminosity dependence is the fact that correlation lengths and amplitudes are almost constant at low luminosities, $M \geq -20.0$. This tendency is seen in observational samples SDSS.19 and SDSS.18, but cannot follow to fainter luminosities due to the absence of very faint galaxies in SDSS luminosity limited samples. In EAGLE and Millennium model galaxy samples this very slow decrease of r_0 and ξ_0 with decreasing luminosity can be followed until very faint galaxies, $M \approx -15.6$ for EAGLE sample, and $M \approx -17.2$ for Millennium sample. This tendency indicates, that very faint galaxies follow the distribution of brighter ones, i.e. faint galaxies are satellites of bright galaxies. The tendency of the clustering dwarf galaxies to form satellites of brighter galaxies is known long ago (Einasto et al. 1974b), see also Wechsler & Tinker (2018). The correlation study confirms this tendency.

4.2. Bias parameters of LCDM and SDSS samples

In Fig. 5 we present the relative bias parameter $b(r, \delta_0)$, for a series of LCDM models with various particle density limits δ_0 . It was calculated using Eq. (5) for the whole range of distances r (separations of galaxies), by dividing correlation functions of unbiased models LCDM. i to the correlation function of the unbiased model LCDM.00. Relative bias parameters for the same biased LCDM models were calculated from power spectra by Einasto et al. (2019a), see Fig. 2 of this paper. Fig. 5 shows that the relative bias parameter has a plateau at $r = 6 h^{-1}$ Mpc, similar to the plateau around $k \approx 0.03 h \text{ Mpc}^{-1}$ of relative power spectra (Einasto et al. 2019a). Both plateaus were used to find amplitudes of correlation functions or power spectra to define respective bias functions. The Figure shows that the amplitude of correlation functions at small distances (pair separations) rises rapidly with the increase of the particle density limit δ_0

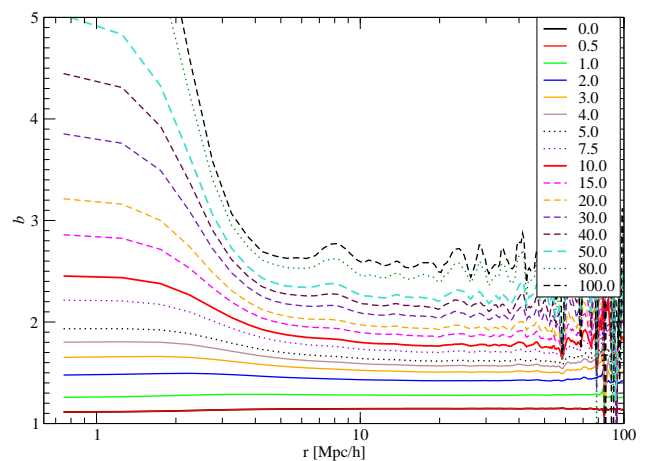


Fig. 5. Relative bias, $b(r)$, of biased LCDM models as functions of the galaxy pair separation r . Particle density limits δ_0 are indicated at symbol labels.

Fig. 5 shows that the relative bias function, $b(r)$, for low values of particle density threshold, $\delta_0 \leq 3$, is almost constant. This suggests that the correlation functions of faint galaxies are almost parallel to the correlation function of matter. The only dif-

ference is in the amplitude. This difference is measured by the bias parameter b , shown in Fig. 5. At these low values of particle density threshold δ_0 the bias parameter is essentially determined by the fraction of matter in the clustered population, i.e. matter, associated with galaxies. This property allows to find absolute bias parameters of biased model samples in respect to matter, as given in Table 1. As expected, bias parameters found from correlation functions are very close to bias parameters of the same model, found from power spectra by Einasto et al. (2019a). For a more detailed discussion of the influence of low-density regions of the density field of matter to correlation function and power spectrum see Einasto et al. (1999).

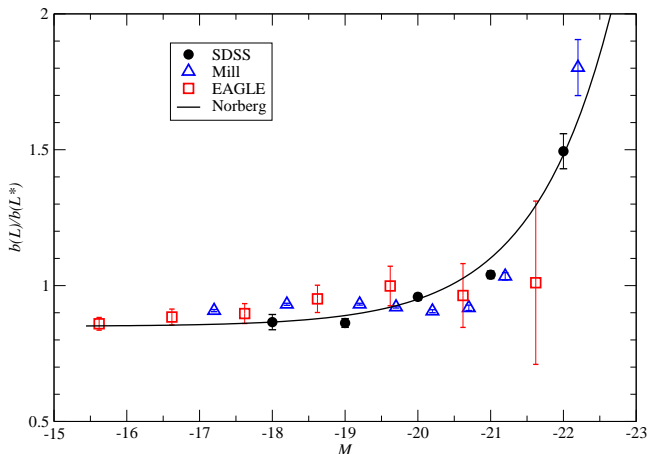


Fig. 6. Relative bias function $b(L)/b(L_*)$ for SDSS, EAGLE and Millennium samples. Solid line shows the relative bias function by Norberg et al. (2001).

In Fig. 6 we show the relative bias function $b(L)/b(L_*)$ for galaxies of various luminosity of SDSS, EAGLE and Millennium samples. The relative bias function was calculated from the relation

$$b(L)/b(L_*) = \sqrt{\xi(6, L)/\xi(6, L_*)}, \quad (7)$$

using amplitudes of correlation functions at the plateau at $r = 6 h^{-1}$ Mpc of samples of luminosity L , divided by the bias value of the same sample at luminosity L_* . This representation is commonly used, here L_* is the characteristic luminosity of samples, it corresponds approximately to the red magnitude $M_r = -20.5$. We see that the relative bias function rises rapidly with the increase of the luminosity over L_* . Such increase of the relative bias parameter at high luminosities was observed already by Norberg et al. (2001), Tegmark et al. (2004a) and Zehavi et al. (2005, 2011). Fig. 6 shows that within errors the relative bias function of the SDSS sample is in agreement with the relative bias function by Norberg et al. (2001). Deviations of Millennium and EAGLE relative correlation functions from the Norberg fit are a bit larger, but within reasonable limits.

Fig. 7 shows the bias parameter $b(\delta_0)$ of the LCDM model as function of δ_0 , see Table 1. This bias parameter relates biased models with unbiased one, i.e. relative to all matter. We see that the bias parameter increases continuously with the increase of the threshold δ_0 , in contrast to the relative bias parameters of the observational and model EAGLE and Millennium galaxy samples, i.e. bias parameters of L galaxies in respect to L_* galaxies, which have flat $r_0(M)$ and $\xi_0(M)$ curves at low luminosities.

This difference can be explained by differences in the distribution of DM particles and dwarf galaxies. Removing low-density particles from the LCDM sample with increasing δ_0 limit

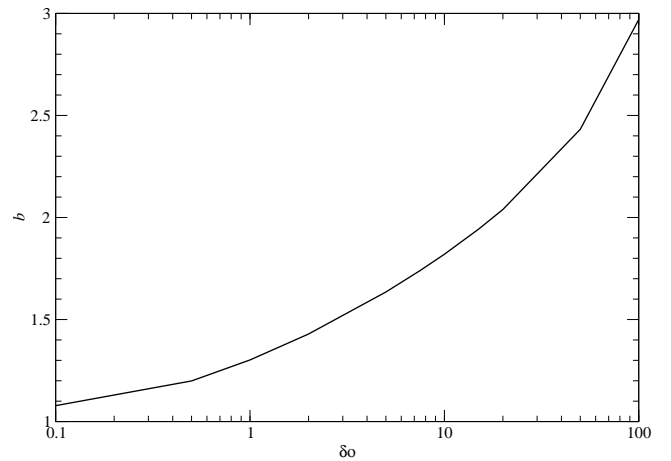


Fig. 7. Bias parameter $b(\delta_0)$ of the LCDM model as function of the particle density threshold δ_0 .

influences the distribution of high-density regions (clusters in terms of the percolation analysis by Einasto et al. (2018)) over the whole volume of the LCDM model. Removing very faint dwarf galaxies from real SDSS or simulated EAGLE and Millennium galaxy samples influences only the structure of halos containing brighter galaxies, but not the structure of voids, since voids do not contain isolated dwarf galaxies. This difference is rather small and does not influence the overall geometrical properties of the cosmic web of real and model samples, as measured by the extended percolation analysis by Einasto et al. (2019a). However, the correlation function is sensitive enough to detect this small difference in the spatial distribution of dwarf galaxies and DM particles in low-density regions.

4.3. Correlation function amplitudes of LCDM and SDSS samples

The amplitudes of correlation functions of biased LCDM samples are systematically higher than respective amplitudes of SDSS galaxy samples, see Tables 1 and 2 and Figs. 4 and 7. Comparison of percolation properties of SDSS and LCDM samples showed that LCDM models with particle density threshold limits $3 \leq \delta_0 \leq 10$ correspond approximately to SDSS samples with absolute magnitude limits $-18.0 \geq M_r \geq -21.0$ (Einasto et al. 2018). Within these selection parameter limits correlation amplitudes of biased LCDM samples can be reduced to the amplitude levels of SDSS samples using an amplitude reduction factor 0.65. The reason of this difference is not clear, one possibility is that our LCDM model has a different σ_8 normalization than real SDSS data.

Fig. 8 shows correlation functions of SDSS samples together with reduced correlation functions of biased model samples LCDM.3, LCDM.10, LCDM.80, as well the correlation function of the whole matter LCDM.00, shown in Figure by black bold dashed line. We see that on medium and large scales, $r \geq 3 h^{-1}$ Mpc, the correlation function of the SDSS.22t sample is very close to the correlation function of the biased model sample LCDM.80. Similarly, correlation function of SDSS.20t and SDSS.21t samples are close to the correlation function of the LCDM.10 sample, and correlation functions of SDSS.18t and SDSS.19t samples are close to correlation function of the LCDM.3 sample. Correlation functions of last two SDSS samples bend down at distance $r \geq 40 h^{-1}$ Mpc, and deviate on larger scales from LCDM samples. This deviation is due to smaller

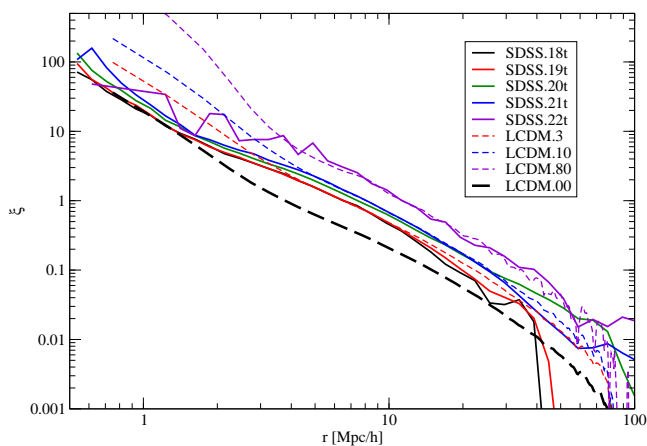


Fig. 8. Correlation functions of SDSS galaxies compared with reduced correlation functions of LCDM samples, using reduction factor 0.65.

volumes of SDSS.18 and SDSS.19 samples, similarly to the behaviour of correlation functions of EAGLE simulation galaxies.

On smaller scales $r \leq 3 h^{-1}$ Mpc correlation functions of LCDM samples have a higher amplitude than correlation functions of corresponding SDSS samples. As discussed above, in this distance range correlation functions of LCDM models reflect the internal structure of DM halos. Inside DM halos the density of DM particles is very high, and all DM particles are present in our samples. This explains the rise of the correlation function of LCDM samples. The number density of visible galaxies in our luminosity limited galaxy samples does not follow this tendency, because most satellite galaxies and cluster members are fainter than the luminosity limit.

4.4. The dependence of fractal properties on the size of the sample

One of the first comparisons of spatial correlation functions of real and model samples was made by Zeldovich et al. (1982). Fig. 2 of this paper compares correlation functions of the observed sample around the Virgo cluster with correlation functions based on Soneira & Peebles (1978) hierarchical clustering model, and hot dark matter (HDM) simulation by Doroshkevich et al. (1982). The observed correlation function has a bend at scale $r \approx 3 h^{-1}$ Mpc. On smaller scales the slope of the correlation function is $\gamma(r) \approx -3$ (fractal dimension $D(r) \approx 0$), present also in the HDM model. On larger scales the slope is much shallower both in the observational and in the HDM model samples. A rapid change of the slope of the correlation function of observational samples at this scale was confirmed by Einasto (1991a,b), Guzzo et al. (1991), Einasto (1992) and Einasto et al. (1997d). Authors emphasised that on smaller scales the slope of structure function, $\gamma(r)$, lies between -1.6 and -2.25 , corresponding to fractal dimensions, $D(r) = 1.4, 0.5$, reflecting the distribution of galaxies in groups and clusters. At larger distances the slope of this function is about -0.8 and reflects the inter-cluster distribution with fractal dimension $D \approx 2.2$.

In the present paper we studied the spatial distribution of real and simulated samples of sizes from hundred to five hundred h^{-1} Mpc. In such large samples fine details of the spatial distribution get smoothed. In earlier similar studies samples of smaller size were available, containing only one or several superclusters. In smaller samples the contrast between clusters and filaments is better seen.

An aspect of the fractal character is the dependence of correlation length on the size of the sample. Einasto et al. (1986) investigated the influence of voids to the distribution of galaxies and found that the correlation length of galaxy samples increases with the increase of the size of the sample. Pietronero (1987) and Calzetti et al. (1987, 1988) explained this result as an evidence for the presence of fractal character of the galaxy distribution. Martínez et al. (2001) investigated the increase of the correlation length with the depth of the sample in more detail. Authors found that the correlation length increases with sample depth for depths up to $30 h^{-1}$ Mpc, using a fractal constructed according to the Soneira & Peebles (1978) model. However, in real galaxy sample of increasing depth over $60 h^{-1}$ Mpc there is no increase of the correlation length with depth.

Another important aspect of the fractal character of the cosmic web is its structure in sub-megaparsec scales, created by tiny filamentary web of DM with sub-voids, sub-sub-voids etc., as discussed among others by Aragon-Calvo et al. (2010a), Aragon-Calvo et al. (2010b) and Aragon-Calvo & Szalay (2013). In this paper we use the spatial resolution of the order of one megaparsec or a bit less, thus fine details of the structure of the DM filamentary web on smaller scales are invisible.

4.5. Zero crossing of correlation functions

Zero crossing of correlation functions is an intrinsic property. Correlation functions are calculated by dividing numbers of galaxy-galaxy pairs to random-random pairs. The integral of the correlation function over the whole space is by definition equal to zero, see Maddox et al. (1996). At small separations the number of neighbours is high. To get a zero total integral the correlation function must be negative at large separations. Since the volume fraction of the high-density regions is small, the negative part of the correlation function can be very close to zero. For this integral constraint zero crossing of correlation functions depends on the volume of samples. In small samples, as the EAGLE sample, zero crossing occurs at relatively small scale, $r_z = 17 h^{-1}$ Mpc. In samples of median size as SDSS.18, SDSS.19 observational samples, and the Millennium sample, zero crossing occurs at scale $r_z \approx 45 h^{-1}$ Mpc. In LCDM model samples it is $r_z \approx 80 h^{-1}$ Mpc, in SDSS.21 and SDSS.22 samples even higher, $r_z \approx 120 h^{-1}$ Mpc. This value reflects probably the actual distance limit where the correlation function of a representative sample of the universe becomes negative.

It is interesting to note that zero crossing of the APM angular correlation function was applied by Maddox et al. (1990, 1996) and Efstathiou et al. (1990) as an argument against the standard CDM model with $\Omega_m = 1$, and favouring a model with cosmological constant, Λ CDM.

Sometimes zero crossing of the correlation function is considered as the transition scale to a homogeneous universe. The definition of a homogeneous universe is not self-evident. Einasto & Gramann (1993) characterised the transition scale to a homogeneous universe using the second derivative of the correlation function, which yields a value $130 h^{-1}$ Mpc. This scale is close to the BAO scale and the scale found by Broadhurst et al. (1990) in the distribution of galaxies in narrow beams, and by Einasto et al. (1994, 1997c, 2016) in the distribution of rich clusters of galaxies. On the other hand, samples of size about $1000 h^{-1}$ Mpc are needed to get a representative sample of very rich superclusters and supercluster complexes of the Sloan Great Wall type, as shown by Klypin & Prada (2019) and Einasto et al. (2019b).

5. Conclusions

We calculated for biased Λ CDM models, and for real and simulated galaxy samples spatial correlation functions of galaxies, and its derivatives, structure functions, and fractal dimension functions. Correlation function and its derivatives are sensitive to the spatial distribution of galaxies in the cosmic web as well as particles within DM halos. Our principal results are as follows.

1. In biased DM models at small distances (separations) correlation functions describe the distribution of particles in DM halos, as given by halo density profiles. The transition from halo to web properties occurs at distance $r \approx 2.25 h^{-1}$ Mpc. In galaxy samples only brightest galaxies in clusters are visible, and the transition from clusters to filaments occurs at distance $r \approx 0.8 h^{-1}$ Mpc for real, and at $r \approx 1.5 h^{-1}$ Mpc for simulated galaxies. On larger separations correlation functions describe the distribution of matter and galaxies in the whole cosmic web.
2. The effective fractal dimension of the cosmic web is a continuous function of distances (particle/galaxy separations). On small separations, $r \leq 2 h^{-1}$ Mpc, the fractal dimension decreases from $D \approx 1.5$ to $D \approx 0$, reflecting the distribution inside halos/clusters. The minimum of the fractal dimension function $D(r)$ near $r \approx 2 h^{-1}$ Mpc is deeper for more luminous galaxies. On medium separations, $2 \leq r \leq 10 h^{-1}$ Mpc, the fractal dimension grows from ≈ 0 to ≈ 2 (filaments to sheets), and approaches at large separations 3 (random distribution).
3. Real and simulated galaxies of low luminosity, $M_r \geq -19$, have almost identical correlation lengths and amplitudes. This is a strong argument indicating that dwarf galaxies are satellites of brighter galaxies, and do not form a smooth population in voids.
4. Correlation functions of most massive DM halos have a bump at $r \approx 8 h^{-1}$ Mpc – a possible hint to regular displacement of clusters along filaments. Correlation functions of most luminous galaxies have a bump at distance $r \approx 2 - 3 h^{-1}$ Mpc, which can be an evidence of the splashback feature in the halo/cluster profile.

Acknowledgements. Our special thanks are to Enn Saar for providing a very efficient code to calculate the correlation function and for many stimulating discussions, and to Ivan Suhhonenko for calculation the Λ CDM model used in this paper. This work was supported by institutional research fundings IUT26-2 and IUT40-2 of the Estonian Ministry of Education and Research, and by the Estonian Research Council grant PRG803. We acknowledge the support by the Centre of Excellence “Dark side of the Universe” (TK133) financed by the European Union through the European Regional Development Fund. The study has also been supported by ICRANet through a professorship for Jaan Einasto. We thank the SDSS Team for the publicly available data releases. Funding for the SDSS and SDSS-II has been provided by the Alfred P. Sloan Foundation, the Participating Institutions, the National Science Foundation, the U.S. Department of Energy, the National Aeronautics and Space Administration, the Japanese Monbukagakusho, the Max Planck Society, and the Higher Education Funding Council for England. The SDSS Web Site is <http://www.sdss.org/>. The SDSS is managed by the Astrophysical Research Consortium for the Participating Institutions. The Participating Institutions are the American Museum of Natural History, Astrophysical Institute Potsdam, University of Basel, University of Cambridge, Case Western Reserve University, University of Chicago, Drexel University, Fermilab, the Institute for Advanced Study, the Japan Participation Group, Johns Hopkins University, the Joint Institute for Nuclear Astrophysics, the Kavli Institute for Particle Astrophysics and Cosmology, the Korean Scientist Group, the Chinese Academy of Sciences (LAMOST), Los Alamos National Laboratory, the Max-Planck-Institute for Astronomy (MPIA), the Max-Planck-Institute for Astrophysics (MPA), New Mexico State University, Ohio State University, University of Pittsburgh, University of Portsmouth, Princeton University, the United States Naval Observatory, and the University of Washington.

References

- Ahn, C. P., Alexandroff, R., Allende Prieto, C., et al. 2014, *ApJS*, 211, 17
Aragon-Calvo, M. A. & Szalay, A. S. 2013, *MNRAS*, 428, 3409
Aragon-Calvo, M. A., van de Weygaert, R., Araya-Melo, P. A., Platen, E., & Szalay, A. S. 2010a, *MNRAS*, 404, L89
Aragon-Calvo, M. A., van de Weygaert, R., & Jones, B. J. T. 2010b, *MNRAS*, 408, 2163
Bagla, J. S., Yadav, J., & Seshadri, T. R. 2008, *MNRAS*, 390, 829
Balian, R. & Schaeffer, R. 1988, *ApJL*, 335, L43
Baryshev, Y. V., Sylos Labini, F., Montuori, M., Pietronero, L., & Teerikorpi, P. 1998, *Fractals*, 6, 231
Baxter, E., Chang, C., Jain, B., et al. 2017, *ApJ*, 841, 18
Berlind, A. A. & Weinberg, D. H. 2002, *ApJ*, 575, 587
Bertschinger, E. 1995, *ArXiv:astro-ph/9506070* [arXiv:astro-ph/9506070]
Blanton, M. R. & Roweis, S. 2007, *AJ*, 133, 734
Borgani, S. 1995, *Phys. Rep.*, 251, 1
Broadhurst, T. J., Ellis, R. S., Koo, D. C., & Szalay, A. S. 1990, *Nature*, 343, 726
Calzetti, D., Einasto, J., Giavalisco, M., Ruffini, R., & Saar, E. 1987, *Ap&SS*, 137, 101
Calzetti, D., Giavalisco, M., & Ruffini, R. 1988, *A&A*, 198, 1
Chacón-Cardona, C. A. & Casas-Miranda, R. A. 2012, *MNRAS*, 427, 2613
Chang, C., Baxter, E., Jain, B., et al. 2018, *The Astrophysical Journal*, 864, 83
Colombi, S., Bouchet, F. R., & Schaeffer, R. 1992, *A&A*, 263, 1
Crain, R. A., Schaye, J., Bower, R. G., et al. 2015, *MNRAS*, 450, 1937
Croton, D. J., Springel, V., White, S. D. M., et al. 2006, *MNRAS*, 365, 11
Diemer, B. & Kravtsov, A. V. 2014, *ApJ*, 789, 1
Doroshkevich, A. G., Shandarin, S. F., & Zeldovich, I. B. 1982, *Comments on Astrophysics*, 9, 265
Efstathiou, G., Sutherland, W. J., & Maddox, S. J. 1990, *Nature*, 348, 705
Einasto, J. 1965, *Trudy Astrofizicheskogo Instituta Alma-Ata*, 5, 87
Einasto, J., Einasto, M., Frisch, P., et al. 1997a, *MNRAS*, 289, 801
Einasto, J., Einasto, M., Frisch, P., et al. 1997b, *MNRAS*, 289, 813
Einasto, J., Einasto, M., Gottlöber, S., et al. 1997c, *Nature*, 385, 139
Einasto, J., Einasto, M., Tago, E., et al. 1999, *ApJ*, 519, 456
Einasto, J. & Gramann, M. 1993, *ApJ*, 407, 443
Einasto, J., Kaasik, A., & Saar, E. 1974a, *Nature*, 250, 309
Einasto, J., Liivamägi, L. J., Suhhonenko, I., & Einasto, M. 2019a, *A&A*, 630, A62
Einasto, J., Saar, E., Kaasik, A., & Chernin, A. D. 1974b, *Nature*, 252, 111
Einasto, J., Saar, E., & Klypin, A. A. 1986, *MNRAS*, 219, 457
Einasto, J., Suhhonenko, I., Liivamägi, L. J., & Einasto, M. 2018, *A&A*, 616, A141
Einasto, J., Suhhonenko, I., Liivamägi, L. J., & Einasto, M. 2019b, *A&A*, 623, A97
Einasto, M. 1991a, *MNRAS*, 250, 802
Einasto, M. 1991b, *MNRAS*, 252, 261
Einasto, M. 1992, *MNRAS*, 258, 571
Einasto, M., Einasto, J., Tago, E., Dalton, G. B., & Andernach, H. 1994, *MNRAS*, 269, 301
Einasto, M., Heinämäki, P., Liivamägi, L. J., et al. 2016, *A&A*, 587, A116
Einasto, M., Tago, E., Jaaniste, J., Einasto, J., & Andernach, H. 1997d, *A&AS*, 123, 119
Gaité, J. 2018, *J. Cosmology Astropart. Phys.*, 2018, 010
Gaité, J. 2019, *Advances in Astronomy*, 2019, 1
Gaité, J., Domínguez, A., & Pérez-Mercader, J. 1999, *ApJL*, 522, L5
Groth, E. J. & Peebles, P. J. E. 1977, *ApJ*, 217, 385
Guzzo, L., Iovino, A., Chincarini, G., Giovanelli, R., & Haynes, M. P. 1991, *ApJL*, 382, L5
Jõeveer, M., Einasto, J., & Tago, E. 1977, *Tartu Astr. Obs. Preprint*, 3
Jõeveer, M., Einasto, J., & Tago, E. 1978, *MNRAS*, 185, 357
Jones, B. J. T., Martínez, V. J., Saar, E., & Einasto, J. 1988, *ApJL*, 332, L1
Kaiser, N. 1984, *ApJL*, 284, L9
Keihänen, E., Kurki-Suonio, H., Lindholm, V., et al. 2019, *A&A*, 631, A73
Klypin, A. & Prada, F. 2019, *MNRAS*, 489, 1684
Klypin, A. A., Einasto, J., Einasto, M., & Saar, E. 1989, *MNRAS*, 237, 929
Kravtsov, A. V., Berlind, A. A., Wechsler, R. H., et al. 2004, *ApJ*, 609, 35
Landy, S. D. & Szalay, A. S. 1993, *ApJ*, 412, 64
Liivamägi, L. J., Tempel, E., & Saar, E. 2012, *A&A*, 539, A80
Limber, D. N. 1953, *ApJ*, 117, 134
Limber, D. N. 1954, *ApJ*, 119, 655
Maddox, S. J., Efstathiou, G., & Sutherland, W. J. 1996, *MNRAS*, 283, 1227
Maddox, S. J., Efstathiou, G., Sutherland, W. J., & Loveday, J. 1990, *MNRAS*, 242, 43
Mandelbrot, B. B. 1982, *The Fractal Geometry of Nature*, ed. Mandelbrot, B. B. Mandelbrot, B. B. 1987, *Astrophysical Letters and Communications*, 36, 1
Martínez, V. J., Jones, B. J. T., Dominguez-Tenreiro, R., & van de Weygaert, R. 1990, *ApJ*, 357, 50
Martínez, V. J., López-Martí, B., & Pons-Bordería, M.-J. 2001, *ApJL*, 554, L5
Martínez, V. J., Paredes, S., & Saar, E. 1993, *MNRAS*, 260, 365

- Martínez, V. J. & Saar, E. 2002, *Statistics of the Galaxy Distribution*, ed. V. J. Martínez & E. Saar (Chapman & Hall/CRC)
- McAlpine, S., Helly, J. C., Schaller, M., et al. 2016, *Astronomy and Computing*, 15, 72
- Navarro, J. F., Frenk, C. S., & White, S. D. M. 1996, *ApJ*, 462, 563
- Norberg, P., Baugh, C. M., Hawkins, E., et al. 2001, *MNRAS*, 328, 64
- Peebles, P. J. E. 1973, *ApJ*, 185, 413
- Peebles, P. J. E. 1975a, *ApJ*, 196, 647
- Peebles, P. J. E. 1975b, *ApJ*, 196, 647
- Peebles, P. J. E. 1980, *The large-scale structure of the universe*, Princeton Series in Physics (Princeton University Press)
- Peebles, P. J. E. 1989, *Physica D Nonlinear Phenomena*, 38, 273
- Peebles, P. J. E. 1998, arXiv e-prints, astro
- Peebles, P. J. E. & Groth, E. J. 1975, *ApJ*, 196, 1
- Peebles, P. J. E. & Hauser, M. G. 1974a, *ApJS*, 28, 19
- Peebles, P. J. E. & Hauser, M. G. 1974b, *ApJS*, 28, 19
- Pietronero, L. 1987, *Physica A Statistical Mechanics and its Applications*, 144, 257
- Press, W. H., Teukolsky, S. A., Vetterling, W. T., & Flannery, B. P. 1992, *Numerical recipes in FORTRAN. The art of scientific computing*
- Schaye, J., Crain, R. A., Bower, R. G., et al. 2015, *MNRAS*, 446, 521
- Seldner, M., Siebers, B., Groth, E. J., & Peebles, P. J. E. 1977, *AJ*, 82, 249
- Shin, T., Adhikari, S., Baxter, E. J., et al. 2019, *Monthly Notices of the Royal Astronomical Society*, 487, 2900
- Soneira, R. M. & Peebles, P. J. E. 1978, *AJ*, 83, 845
- Springel, V. 2005, *MNRAS*, 364, 1105
- Springel, V., White, S. D. M., Jenkins, A., et al. 2005, *Nature*, 435, 629
- Szapudi, I., Pan, J., Prunet, S., & Budavári, T. 2005, *ApJL*, 631, L1
- Szapudi, I., Prunet, S., Pogosyan, D., Szalay, A. S., & Bond, J. R. 2001, *ApJL*, 548, L115
- Tegmark, M., Blanton, M. R., Strauss, M. A., et al. 2004a, *ApJ*, 606, 702
- Tegmark, M., Strauss, M. A., Blanton, M. R., et al. 2004b, *Phys. Rev. D*, 69, 103501
- Tempel, E., Einasto, J., Einasto, M., Saar, E., & Tago, E. 2009, *A&A*, 495, 37
- Tempel, E., Kipper, R., Saar, E., et al. 2014a, *A&A*, 572, A8
- Tempel, E., Tamm, A., Gramann, M., et al. 2014b, *A&A*, 566, A1
- Totsuji, H. & Kihara, T. 1969, *PASJ*, 21, 221
- van de Weygaert, R., Shandarin, S., Saar, E., & Einasto, J., eds. 2016, *IAU Symposium, Vol. 308, The Zeldovich Universe: Genesis and Growth of the Cosmic Web*
- Wang, J., Bose, S., Frenk, C. S., et al. 2019, arXiv e-prints, arXiv:1911.09720
- Wechsler, R. H. & Tinker, J. L. 2018, *ARA&A*, 56, 435
- White, S. D. M. & Rees, M. J. 1978, *MNRAS*, 183, 341
- Zehavi, I., Weinberg, D. H., Zheng, Z., et al. 2004, *ApJ*, 608, 16
- Zehavi, I., Zheng, Z., Weinberg, D. H., et al. 2011, *ApJ*, 736, 59
- Zehavi, I., Zheng, Z., Weinberg, D. H., et al. 2005, *ApJ*, 630, 1
- Zeldovich, Y. B., Einasto, J., & Shandarin, S. F. 1982, *Nature*, 300, 407